Oxygen permeation in symmetric and asymmetric $La_{0.2}Sr_{0.8}Fe_{0.8}Ta_{0.2}O_{3-\delta}$ membranes

Jonas Gurauskis [‡*], Ørjan Fossmark Lohne, Dan Stræte Lagergren, Espen Tjønneland Wefring, Kjell Wiik[*].

Department of Materials Science and Engineering, Norwegian University of Science and Engineering, Sem Sælandsvei 12, NO-7491, Trondheim, Norway.

Abstract

$La_{0.2}Sr_{0.8}Fe_{0.8}Ta_{0.2}O_{3-\delta}$ (LSFT) is a mixed ionic electronic conductor (MIEC) at elevated temperatures and as such a candidate material for applications both in syn-gas synthesis and as electrodes in solid oxide fuel cells (SOFC). This study addresses the variation in oxygen permeation rates for LSFT symmetric- and asymmetric-membranes at temperatures between 800 and 1000 ^{o}C with and without surface modification. The surface was strutured in two different scales, macro (porous LSFT-layer) and micro (acid etching). The asymmetric membranes showed a significant variation in permeation rate with surface treatment with increasing rate in the sequence from non-treated to macro-structured and finally micro structured, corresponding to oxygen permeation being controlled by surface exchange and gas diffusion. It was found that the permeation rate was sensitive to the gas sweep rate when H_2-mixtures was introduced on the permeate side, which was rationalized by adsorption of H_2O-molucules on the surface hampering the exchange of oxygen.

Keywords: Oxygen permeation, perovskite, asymmetric membrane, surface modification, stability.

[‡] Current address: Department of Energy Conversion and Storage, Technical University of Denmark, Frederiksborgvej 399, 4000 Roskilde, Denmark.
*- Corresponding authors: kjell.wiik@ntnu.no (+47 73594082), jogu@dtu.dk (+45 24649403).

Introduction

Mixed oxygen-ionic and electronic conducting (MIEC) perovskite oxides (ABO_3) can be used to separate oxygen from air at temperatures above 700 °C [1-3]. Hence, given sufficient mixed conductivity in combination with adequate chemical and mechanical stability; they could efficiently be used as dense ceramic membrane reactors providing pure oxygen to the chemical industry. An even more demanding application is the production of syn-gas ($CO+H_2$) by partial oxidation of natural gas [1,2,4,5], in this case the mixed conductor must be stable at both high temperatures and severe reducing conditions.

One group of promising MIEC-materials with high oxygen permeability is the perovskite system based on lanthanum-strontium ferrite (LSF) [6]. The enhanced oxygen ionic conductivity in these materials is basically due to high concentration of oxygen vacancies.

There are a number of different approaches to stabilize LSF, and from an oxygen transport point of view we both want to suppress ordering of oxygen vacancies (formation of brownmillerite type structure) as well as avoid decomposition [6-9]. In a previous work [10], we investigated how oxygen transport properties and stability were affected by substituting the B-site ($La_{0.2}Sr_{0.8}Fe_{0.8}B_{0.2}O_{3-\delta}$) with aliovalent cations with different radii. The difference in apparent stability was assessed by temperature programmed reduction (TPR) and the highest stability was observed for B-site substitution with Al^{3+} and Ta^{5+}, respectively. It was also observed that all B-site substitutions (Al, Ga, Ti, Cr, Zr, Nb and Ta) suppressed the formation of an oxygen vacancy ordered phase (brownmillerite). In light of these results and the ones reported by Diethelm et al. [8], the $La_{0.2}Sr_{0.8}Fe_{0.8}Ta_{0.2}O_{3-\delta}$ perovskite system was selected for further evaluation as a high flux, structurally optimized, dense ceramic membrane.

One obvious way to improve the oxygen flux is to decrease the membrane thickness below the critical thickness such that the oxygen permeation rate is solely controlled by surface exchange processes. Even higher fluxes may be obtained by using either a catalytic layer [4,11-13] or simply increasing the surface area available for surface exchange to take place [14-17], or both.

In this work, the applicability of membranes with composition $La_{0.2}Sr_{0.8}Fe_{0.8}Ta_{0.2}O_{3-\delta}$ operating at moderate ($\approx 10^{-2}$ atm) and low ($\approx 10^{-16}$ atm) oxygen partial pressures at the permeate side will be addressed. For this purpose we employed varying thickness of both bulk and asymmetric membrane structures, with and without surface area modification at the sweep (permeate) side to study the effect on the resulting oxygen flux.

Material and methods

$La_{0.2}Sr_{0.8}Fe_{0.8}Ta_{0.2}O_{3-\delta}$, further abbreviated as LSFTa, powder was obtained by the method of spray pyrolysis [10]. Bulk reference membranes were made by uniaxial pressing of LSFTa powder into disk shaped pellets followed by sintering at 1230 °C for 2 h. Obtained bulk pellets were grinded and polished using final mesh of 1200 to two desired thicknesses: 1000 μm and 500 μm. Asymmetric membranes were prepared by using porous LSFTa powder substrates, dip coating to form the dense layer on top followed by sintering. Full description of asymmetric membrane processing route is given elsewhere [17].

The surface at the membrane (permeate) side of the asymmetric membrane was modified in two different ways, so called macro- and micro-structuring, respectively: Macro-structuring was obtained by applying an extra LSFTa porous layer on top of the surface. For this purpose the deposition of LSFTa colloidal suspension with starch as a pore former was done. For better adhesion, the deposition of porous layer was done before the final sintering step, on top of presintered (1100 °C, dwell 2 h) dense membrane layer. Micro-structuring was obtained by surface etching. For this purpose the membrane was exposed to 6M HCl for 10 minutes at room temperature.

Phase purity after sintering and prior to permeation was checked by means of X-ray diffraction using Bruker D8 diffractometer. Microstructures of as processed and tested membranes were assessed by Hitachi S3500N scanning electron microscope (SEM). Elemental analysis of observed compounds was performed at 15 kV using the energy dispersive X-ray spectrometry (EDS).

Experimental

For oxygen flux measurements the disk shaped LSFTa membranes were sealed to the alumina support tubes at ~1058 °C using gold gaskets to form two gas chambers. The complete structure of the oxygen permeation cell is described in more detail elsewhere [17]. The effective membrane area after sealing was 1.1 cm^2. Prior to measurements, gas tightness of the gold seals and the membrane system was evaluated at 800 °C using He(g) (6.0 gas purity). He(g) was supplied to the feed side at ~2.1 atm pressure and Ar(g) was supplied to the permeate (sweep) side at ~1.1 atm pressure. Presence of He in the sweep gas was assessed by

gas chromatography (Varian Micro-GC CP4900) using Ar as a carrier gas. Leak detection was performed routinely to assure the seal tightness and absence of pinholes/gas leaks within the membrane system at high temperatures.

Variation in oxygen partial pressure on the permeate side was achieved by sweeping Ar(g) (5.0 gas purity) at flow rates between 50 and 860 Nml/min, where NmL is volume at 1 atm and 22 ^{o}C. In order to extend the oxygen partial pressure range on the permeate side, mixing of Ar sweep gas with pure O_2 (5.0 gas purity) as well as mixtures of 5% H_2 in Ar (5.0 gas purity) were applied. A constant flow of 100 Nml/min of pure O_2 (5.0 gas purity) was supplied on the feed side during all experiments. The total pressure on both sides of the membrane was ~1.1 atm during all experiments, and the unit NmL/min refers to mL/min measured at 1 atm and 25 °C.

Measurements were carried out between 800 and 1000 °C, leaving 4–6 h for stabilization at each set of experimental parameters. A gas chromatograph with Ar as a carrier gas determined the O_2 concentration in the sweep gas. Calibration of the gas chromatograph was routinely done by using O_2 and H_2 reference gases.

Calculation of bulk diffusion

The oxygen transport rate through a MIEC perovskite membrane may depend on both solid-state diffusion and oxygen surface exchange. If the flux of oxygen is entirely controlled by solid-state diffusion (bulk diffusion), the rate of oxygen permeation can be estimated using the Wagner equation. Provided that oxygen nonstoichiometry (δ), chemical diffusion coefficient (D_{chem}) and oxygen vacancy thermodynamic factor (W_V) at the given temperature all are available as a function of pO_2. The oxygen flux can be calculated numerically using the following form of Wagner´s equation [2]:

$$jO_2 = -\frac{D_V}{4 \cdot L} \int_{\ln pO_{2\,low}}^{\ln pO_{2\,high}} c_V \cdot d\ln pO_2 \qquad (1)$$

where D_V is the oxygen vacancy diffusion coefficient ($D_V=D_{chem}/W_V$), L is membrane thickness and c_V is the concentration of oxygen vacancies $c_V = \delta / V_m$ (V_m being molar volume of the perovskite). This form of Wagner´s equation can be used to estimate the oxygen flux throughout the membrane only if the following assumptions are correct: the ionic

conductivity is much smaller than the electronic conductivity, all oxygen vacancies are free and contribute to ionic transport and, finally, D_V is constant over the experimental range of oxygen nonstoichiometry at the temperature in question. In our case LSFTa composition has V_m=36.24 cm^3/mol and it is proved to be constant within current experimental conditions [10]. The variation in c_v with respect to pO_2 is based on data given by Lohne et al. [18] and is, for simplicity, converted to a 2nd degree polynomial, taking into account that at 900 °C and $10^{-16} \le P_{O_2}\,(atm) \le 1$ c_v is well described by Eq. (2):

$$c_v = aP_{O_2}^2 + bP_{O_2} + c \tag{2}$$

and substitution into Eq. (1) gives:

$$J_{O_2} = -\frac{D_V}{4L}\int_{P_{O_2,low}}^{P_{O_2,high}} \left(aP_{O_2}^2 + bP_{O_2} + c\right) d\ln P_{O_2} \tag{3}$$

Solving the integral in Eq. (3) gives the following final expression for the oxygen flux in terms of pO_2, D_V and L:

$$J_{O_2} = -\frac{D_V}{4L}\Big|_{P_{O_2,low}}^{P_{O_2,high}} \left(\frac{a}{2}P_{O_2}^2 + bP_{O_2} + c\ln P_{O_2}\right) \tag{4}$$

Results

Dense, thick film (≥500 μm) membranes reached 98 % of theoretical density after sintering at 1230 °C for 2 h. Porous supports of asymmetric membranes had the apparent porosity of ~34 % and a defect free dense layer with thickness of ~25 μm as illustrated in Figs. 1a-b. The inset in Fig. 1b shows a submicron grain size at the surface, typically between 500 and 600 nm. Macro- and micro-structurally modified surfaces of permeate side are shown in Figs. 1c-d.

The oxygen fluxes as a function of oxygen partial pressure measured at varying temperatures for thick (~500 μm and ~1000 μm) and asymmetric (~25 μm) LSFTa membranes are shown in Fig. 2. In all cases oxygen flux increased with temperature and difference in oxygen partial pressure (driving force) between feed and permeate side. The trend lines were used to establish the ratio between the oxygen fluxes for asymmetric LSFTa membranes with different surface finish, and are summarized in Table 1. Oxygen flux rates as high as ~8.8 NmL×min-

$^{1}\times cm^{-2}$ were obtained for both macro- and micro-structured asymmetric membranes at 1000 °C. Based on available nonstoichiometry data for LSFTa composition [18] and using Eq. 4, one can estimate the variation in flux (jO_2) in terms of log pO_2 at a given temperature. Figure 3 shows the best fit for oxygen flux for thick membranes with L equal to 500 and 1000 μm at 900°C obtained for $D_V=1.2\cdot10^{-5}$ cm^2/s.

The Arrhenius-type plot of the oxygen permeation fluxes for the thick (≥500 μm), 25 μm asymmetric and modified surface membranes measured between 800 and 1000 °C at a fixed partial pressure of 10^{-2} atm at the permeate side is given in Fig. 4. Estimated apparent activation energies, $E_{a,a}$, are summarized in Table 2. Both thick membranes (500 and 1000 μm) show $E_{a,a}\approx$ 80 kJ/mol throughout the whole temperature range measured, while the macro-structured asymmetric membrane showed $E_{a,a}\approx$ 37 kJ/mol in the same temperature interval. However, both the asymmetric membrane (non structured surface) and micro-structured asymmetric membrane changed activation energy from approx. 112 kJ/mol below 900°C to about 33 kJ/mol above 900°C, suggesting a shift in rate controlling process.

The oxygen flux for all membranes at 900 °C and at a fixed partial pressure of 10^{-2} atm at the permeate side versus the thickness of the membrane are shown in Fig. 5. Oxygen flux is seen to be proportional to reciprocal thickness (1/L) for thick membranes, consistent with bulk diffusion being rate controlling (Cf. Eq. 1). However, the asymmetric membranes with 25 μm dense layer (non structured, macro- and micro-structured) are seen to deviate significantly from the 1/L-proportionality indicating that permeation becomes controlled by surface exchange. It is also evident that for the asymmetric membranes (thickness 25 μm) increasing flux is observed as the surface is changed from non-treated to macro-structured and micro-structured, respectively, clearly demonstrating the importance of surface structure in this regime.

Micro-structured asymmetric membranes were also exposed to 5% hydrogen (rest Ar) at the permeate side for 100 hours at 900 °C and the results are given in Fig. 6. It is seen, Fig. 6a, that there is a significant reduction in oxygen flux when the 5% H_2-mixture is introduced at a flow rate of 100 NmL/min (corresponding to $pO_2<10^{-2}$ atm) and that the flux is virtually independent of flow rate until approx. 137 NmL/min. In the same flow regime it is also evident that all the H_2(g) fed to the permeate side, Fig. 6b, is consumed according to the reaction:

$$H_2(g) + 1/2O_2(g) \rightarrow H_2O(g) \quad (5)$$

A further increase in the gas flow rate beyond 137 mL/min (Fig. 6a) is seen to enhance the flux quite significantly to almost 6 mL/min·cm^{-2} at 285 mL/min corresponding to $pO_2 \sim 10^{-15}$ atm. At the same time Fig. 6b shows that an increasing fraction of $H_2(g)$ fed to the permeate side is not consumed at flow rates > 137 mL/min. Possible reasons for this behaviour will be further discussed in the next section.

After 100 h of operation time under hydrogen the sweep gas was changed back to argon. The permeation rate decreased by ~6 % compared with oxygen flux values measured before exposure to hydrogen (Fig. 6a).

Membranes were un-mounted by melting the gold seals and subsequently cooled at 5 °C/min. The asymmetric membranes showed full structural integrity while the thick reference membranes cracked during cooling due to chemical expansion. The permeate-side surface of all membranes showed a slight colour change due to prolonged exposure to gas flow at elevated temperature, but no formation of secondary phases was detected. Polished cross-sections of all membranes was analysed by SEM/BSE and no secondary phases were observed. However, on the feed side of the thick reference membranes, formation of a strontium/iron-rich phase was detected (Fig. 7a-b), and EDS (spectrum 2, Fig. 7b) confirmed the formation of $SrFe_{12}O_{19}$ phase.

Discussion

Surface structure. As seen from Figs. 1a-b, a defect free and relatively smooth surface finish was achieved at oxygen permeate side. The use of LSFTa powder with small primary particles obtained by spray pyrolysis resulted in a fine grained microstructure with grain size distribution below 1 μm (inset Fig. 1b). Macro-structural surface modification by deposition of a porous layer on top of the dense membrane layer resulted in a 10-15 μm thick highly porous “coral type” surface structure at the permeate side (Fig. 1c). Micro-structural dense membrane layer modification (acid etched) at oxygen permeate side increased the surface area of each single grain (Fig. 1d) and accordingly generated significantly more surface available for oxygen exchange reactions to take place. The resulting surface morphology is

due to the more pronounced acid etching taking place at grain boundaries in contrast to the grains itself. The x-ray analysis of the acid etched surface showed identical LSFTa composition compared to untreated, confirming the absence of preferential cation etching and possible deviation from nominal LSFTa stoichiometry.

Interpretation of oxygen flux. It is obvious from Fig. 2 that assessment of oxygen flux is hampered with some uncertainty, nevertheless there seems to be a quite strong linear relationship between flux and log pO_2 for all samples and temperatures. The best linear fit is included as broken lines in Figs. 2a-c, and in case of asymmetric membranes, the interception with ordinate (oxygen flux) is designated as J_1, J_2, J_3, for 25 μm, 25 μm macro- and 25 μm micro- structured membranes, respectively. The ratio between these fluxes is tabulated in Tab. 1 and will be discussed in the following. It is clear that both thick membranes (500 and 1000 μm) show low permeation rates compared with the asymmetric membranes and it is reasonable to assume that the flux is controlled by bulk diffusion. The presence of the 1/L linear relationship for thick films is confirmed by data presented in Fig. 5, where oxygen flux data for 900°C at fixed driving force is presented. Based on the numerical flux values reported for the thick membranes at 900°C (Fig. 2b) we fitted the solution of Wagner´s equation, Eq. (4), to the experimental data using the vacancy diffusion coefficient, D_V, as a variable. The results are given in Fig. 3, and there is a close fit for $D_V=1.2\cdot10^{-5}$ cm²/s. This corresponds well with Lohne et al. [19, pp. 153-155] reporting $D_v=9.1\cdot10^{-6}$ cm²/s based on electrical conductivity relaxation (ECR) at 900 °C, and utterly support that bulk diffusion is rate controlling for thick membranes. Fig. 2 also shows that there is a significant increase in flux between thick and asymmetric membranes. The thickness of the asymmetric membranes was fixed at 25 μm, and we can clearly see from Fig. 5 that the linear relationship between flux and 1/L at 900°C is no longer fulfilled and suggests that the flux is now controlled by reactions taking place at the surface. With reference to Tab. 1 it seems to be a clear trend that the ratio between J_3 (micro structured) and J_1 (untreated surface) is constant at 1.6 independent of temperature, which indicates that surface reactions at the permeate side is rate controlling and that the surface area increase by a factor of 1.6 when micro-structuring (etching). The same tendency, although more scattered data, is also observed for the macro-structured (J_2) surface reflected by the enhanced ratio between J_2 and J_1 given in Tab. 1.

Interpretation of (apparent) activation energy, E_a. The apparent activation energy values for oxygen flux through thick membranes is just below 80 kJ/mol (Fig. 4 and Tab. 2) and are

comparable with values published by other authors. Bayraktar et al. [9] reported $E_{a,a}$ = 93 (11) kJ/mol for $La_{0.5}Sr_{0.5}Fe_{0.9}Ta_{0.1}O_{3-\delta}$ the same as Chen et al. [19] who reported $E_{a,a}$ = 93 (2) kJ/mol for $La_{0.4}Sr_{0.6}Fe_{0.8}Co_{0.2}O_{3-\delta}$. Both authors specify that these activation energies correspond to the oxygen bulk diffusion controlled regime supporting our assumption that the thick membranes are controlled by bulk diffusion.

Both the micro structured- and non-structured asymmetric membranes showed activation energies around 110 kJ/mol between 800 and 900°C (Fig. 4 and Tab. 2). These E_a values are comparable with the ones observed for $La_{0.5}Sr_{0.5}Fe_{0.9}Ta_{0.1}$ $O_{3-\delta}$ composition membranes reported by Bayraktar et al. [9] ($E_{Bayraktar}$=121kJ/mol), where the limiting factor for oxygen transport also was attributed to surface exchange reactions. In our case both membranes show a significant shift to lower activation energy, ~33 kJ/mol, at temperatures above ~900 °C. This is a rather low activation energy and may correspond to gas diffusion limitations at permeate side. This is even more pronounced for the highly porous "coral type" structure (Fig. 1c) showing a low (~37 kJ/mol) activation energy at all temperatures, which may be due to insufficient gas sweep at permeate side and gas diffusion control [21]. Permeation in 5% hydrogen. The change in sweep gas from argon to 5 % hydrogen in argon reduced the resulting oxygen flux significantly for micro-structural asymmetric membrane at 900 °C (Fig. 6a). Intuitively one would expect enhanced flux due to increased driving force. Nevertheless, the oxygen flux is practically independent of the partial pressure of oxygen between approx. 10^{-2} (100 NmL/min) and 10^{-14} atm (137 NmL/min). However, increasing the flow of 5% hydrogen beyond 137 NmL/min do increase the permeation flux of oxygen and at 285 NmL/min (pO_2=10^{-15} atm) the flux is almost 6 NmL/min·cm^2. Fig. 6b (broken line) describes the consumption of H_2(g) according to Eq. (5) based on the measured oxygen flux, while the solid line corresponds to the actual feed rate of H_2(g). It is obvious that all hydrogen is consumed until a feed rate of approx. 4.75 μmol/s (corresponding to a sweep gas rate of 137 NmL/min), and that an increasing amount of hydrogen pass the membrane unreacted at flow rates beyond 137 NmL/min. Although the presence of hydrogen potentially may define a low pO_2 it is equally obvious that its presence somehow hampers the surface exchange kinetics significantly. It is tempting to claim that rather than the hydrogen, the problem is the formation of H_2O(g) which, due to its large dipole moment, may adsorb strongly to charged sites at the surface such as e.g. oxygen vacancies. Vacancies may be active sites for adsorption

of hydrogen followed by reaction according to Eq. (3). Hence, if water is occupying active sites this may explain major decrease in flux as hydrogen is introduced. Why the flux eventually increase at sufficient high flow of sweep gas, may be due to an increased rate of diffusive transport of $H_2O(g)$ away from the surface caused by the thinner gas film layer at the surface, which will steadily decrease with increasing flow rate. After changing the sweep gas back to argon, after 100 h operation at reducing conditions and 900 ^oC, the membranes basically regained the oxygen flux values measured before exposure to hydrogen. The observed ~6 % reduction is considered to be within the experimental accuracy of the method. However, considerable longer tests are necessary to establish the typical long term stability of this material system at elevated temperatures and reducing conditions.

Kinetic demixing. Since the feed side of the membrane is quite oxidative while the permeate side is rather reducing there will in principle always be a driving force for the migration of cations where the most mobile cation will migrate at the highest rate. This phenomenon is usually described as kinetic demixing and it is apparent that it has taken place in the thick membranes (500 and 1000 μm) with the formation of $SrFe_{12}O_{19}$ (hexaferrite) at the feed side for ≥500 μm membranes exposed for ~ 550 h at temperatures between 800 and 1000 °C (Fig. 7a-b). The observed formation of hexaferrite for thick membranes at the feed side have been reported previously by Lein et al. [20] for $La_{0.5}Sr_{0.5}Fe\ O_{3-\delta}$ membranes after ~720 h of operation time at 1150 °C. Diethelm et al. [8] reported that for $La_{0.5}Sr_{0.5}Fe_{0.9}Ta_{0.1}O_{3-\delta}$ membrane Sr-rich phases were detected at the feed side after ~ 2000 h of operation time. In all cases, the decomposition was limited to nearby surface areas at the feed side. A more detailed study addressing the phenomena of kinetic demixing will be reported in a subsequent paper.

Conclusions

Effect of membrane geometries (symmetric and asymmetric) and permeate side structure modifications (only asymmetric) on oxygen transport properties of $La_{0.2}Sr_{0.8}Fe_{0.8}Ta_{0.2}O_{3-\delta}$ based membrane was addressed. As expected, the oxygen flux is considerably improved when the thickness of the membrane layer is reduced to the level where flux is controlled by surface reactions. For the asymmetric membranes further oxygen flux improvements were achieved

by simply increasing the surface area available for oxygen exchange to take place at the permeate side. The surface area modifications were done at different micro- and macro-scales and at 900 ^{o}C a significant increase in permeation rate was observed in the sequence from non-treated to macro-structured and finally micro structured.

At high temperatures (>900°C) apparent activation energies between 30 and 40 kJ/mol were observed for all asymmetric membranes, indicating that gas diffusion becomes rate controlling. At lower temperatures the activation energies were typically between 105 and 118 kJ/mol consistent with representative values for surface exchange processes reported elsewhere.

The applicability of $La_{0.2}Sr_{0.8}Fe_{0.8}Ta_{0.2}O_{3-\delta}$ based membranes was addressed for operation at low ($\approx 10^{-16}$ atm) oxygen partial pressures, where sweep at the permeate side was performed using 5% H_2 in Ar. It was found that the permeation rate was sensitive to the gas sweep rate, which was rationalized by adsorption of H_2O-molecules on the surface hampering the exchange of oxygen. Long time operation (> 100 hours) of the asymmetric membranes at high temperatures and reducing conditions did not seem to affect their performance; they showed overall good reproducibility and post analysis did not reveal any detrimental reactions or structural changes.

However, formation of a secondary phase ($SrFe_{12}O_{19}$) was observed on the feed side of thick membranes after testing for ~ 550 h at temperatures between 800 and 1000 °C. The formation of the secondary phase at the high pO_2 side was attributed to kinetic demixing and is previously reported for perovskite membranes of similar composition.

Acknowledgements

Funding provided by the Norwegian Research Council (NFR), FRINAT-project no. 191358: "The kinetics of surface exchange reactions in oxide based mixed conductors at reducing conditions and high temperatures", is acknowledged.

References:

[1] Steele BCH. Oxygen ion conductors and their technological applications. Mater. Sci. Eng. B 1992;13:79–87. DOI:10.1016/0921-5107(92)90146-Z.

[2] Bouwmeester HJM. Dense ceramic membranes for methane conversion. Catal. Today 2003;82:141–50. DOI:10.1016/S0920-5861(03)00222-0.

[3] Baumann S, Meulenberg WA, Buchkremer HP. Manufacturing strategies for asymmetric ceramic membranes for efficient separation of oxygen from air. J Eur Ceram Soc 2013;33:1251–61. DOI:10.1016/j.jeurceramsoc.2012.12.005.

[4] Fang S, Chen C, Winnubst L. Effect of microstructure and catalyst coating on the oxygen permeability of a novel CO_2-resistant composite membrane. Solid State Ionics 2011;190:46–52. DOI:10.1016/j.ssi.2011.03.009.

[5] Bayraktar D, Clemens F, Diethelm S, Graule T, Van herle J, Holtappels P. Production and properties of substituted $LaFeO_3$-perovskite tubular membranes for partial oxidation of methane to syngas. J. Eur. Ceram. Soc. 2007;27:2455–61. DOI:10.1016/j.jeurceramsoc.2006.10.004.

[6] Tsipis EV, Patrakeev MV, Kharton VV, Yaremchenko AA, Mather GC, Shaula AL, et al. Transport properties and thermal expansion of Ti-substituted $La_{1-x}Sr_xFeO_{3-\delta}$. Solid State Sci. 2005;7:355–65. DOI:10.1016/j.solidstatesciences.2005.01.001.

[7] Atkinson A, Ramos TMGM. Chemically-induced stresses in ceramic oxygen ion-conducting membranes. Solid State Ionics 2000;129:259–69. DOI:10.1016/S0167-2738(99)00331-8.

[8] Diethelm S, Bayraktar D, Graule T, Holtappels P, Van herle J. Improved stability of $La_{0.5}Sr_{0.5}FeO_3$ by Ta-doping for oxygen separation membrane application. Solid State Ionics 2009;180:857–60. DOI:10.1016/j.ssi.2009.02.001.

[9] Bayraktar D, Diethelm S, Graule T, Van Herle J, Holtappels P. Properties of B-site substituted $La_{0.5}Sr_{0.5}FeO_{3-\delta}$ perovskites for application in oxygen separation membranes. J. Electroceramics 2009;22:55–60. DOI:10.1007/s10832-008-9428-z.

[10] Lohne ØF, Gurauskis J, Phung TN, Einarsrud M-A, Grande T, Bouwmeester HJM, et al. Effect of B-site substitution on the stability of $La_{0.2}Sr_{0.8}Fe_{0.8}B_{0.2}O_{3-\delta}$, B=Al, Ga, Cr, Ti, Ta, Nb. Solid State Ionics 2012;225:186–9. DOI:10.1016/j.ssi.2012.02.061.

[11] Teraoka Y, Honbe Y, Ishii J, Furukawa H, Moriguchi I. Catalytic effects in oxygen permeation through mixed-conductive LSCF perovskite membranes. Solid State Ionics 2002;152-153: 681–7. DOI:10.1016/S0167-2738(02)00409-5.

[12] Figueiredo FM, Kharton V V, Viskup AP, Frade JR. Surface enhanced oxygen permeation in $CaTi_{1-x}Fe_xO_{3-\delta}$ ceramic membranes. J. Memb. Sci. 2004;236:73–80. DOI: 10.1016/j.memsci.2004.02.008.

[13] Tan X, Wang Z, Liu H, Liu S. Enhancement of oxygen permeation through $La_{0.6}Sr_{0.4}Co_{0.2}Fe_{0.8}O_{3-\delta}$ hollow fibre membranes by surface modifications. J. Memb. Sci. 2008;324:128–35. DOI: 10.1016/j.memsci.2008.07.008.

[14] Kusaba H, Shibata Y, Sasaki K, Teraoka Y. Surface effect on oxygen permeation through dense membrane of mixed-conductive LSCF perovskite-type oxide. Solid State Ionics 2006;177:2249–53. DOI:10.1016/j.ssi.2006.05.038.

[15] Chen T, Zhao H, Xie Z, Lu Y, Xu N. Improved oxygen permeability of $Ce_{0.8}Sm_{0.2}O_{2-\delta}$-$PrBaCo_2O_{5+\delta}$ dual-phase membrane by surface-modifying porous layer. Int. J. Hydrogen Energy 2012;37:19133–7. DOI:10.1016/j.ijhydene.2012.09.144.

[16] Kida T, Ninomiya S, Watanabe K, Yamazoe N, Shimanoe K. High oxygen permeation in $Ba_{0.95}La_{0.05}FeO_{3-\delta}$ membranes with surface modification. ACS Appl. Mater. Interfaces 2010;2:2849–53. DOI: 10.1021/am100524k.

[17] Gurauskis J, Lohne ØF, Wiik K. $La_{0.2}Sr_{0.8}Fe_{0.8}Ta_{0.2}O_{3-\delta}$ based thin film membranes with surface modification for oxygen production. Solid State Ionics 2012;225:703–6. DOI:10.1016/j.ssi.2012.02.053.

[18] Lohne ØF, Phung TN, Grande T, Bouwmeester HJM, Hendriksen P V., Sogaard M, et al. Oxygen Non-Stoichiometry and Electrical Conductivity of $La_{0.2}Sr_{0.8}Fe_{0.8}B_{0.2}O_{3-\delta}$, B = Fe, Ti, Ta. J. Electrochem. Soc. 2013;161:F176–84. DOI:10.1149/2.001403jes.

[19] Chen C -s., Zhang Z -p., Jiang G -s., Fan C -g., Liu W, Bouwmeester HJM. Oxygen Permeation through $La_{0.4}Sr_{0.6}Co_{0.2}Fe_{0.8}O_{3-\delta}$ membrane. Chem. Mater. 2001;13:2797–800. DOI: 10.1021/cm000809a.

[20] Lein H, Wiik K, Grande T. Kinetic demixing and decomposition of oxygen permeable membranes. Solid State Ionics 2006;177:1587–90. DOI:10.1016/j.ssi.2006.03.001.

Table

Table 1. Ratio between the oxygen flux values at moderate oxygen pressure range (down $10^{-2,5}$ atm) for asymmetric LSFTa membranes.

Flux / T (°C)	J_2/J_1	J_3/J_1
800	1.8	1.6
900	1.2	1.6
1000	1.6	1.6

Table 2. Apparent activation energy values (Ea,a) as a function of temperature segments. Values obtained at fixed oxygen partial pressure difference of 10^{-2} atm.

Membrane thickness and surface modification	Temperature range (°C)	Ea,a (kJ/mol)
1000 µm	800 – 1000	78 (3)
500 µm		77 (5)
25 µm macro-structured		37 (10)
25 µm	800-900	105
	900-1000	34
25 µm micro-structured	800-900	118
	900-1000	32

Figure 1a
Click here to download high resolution image

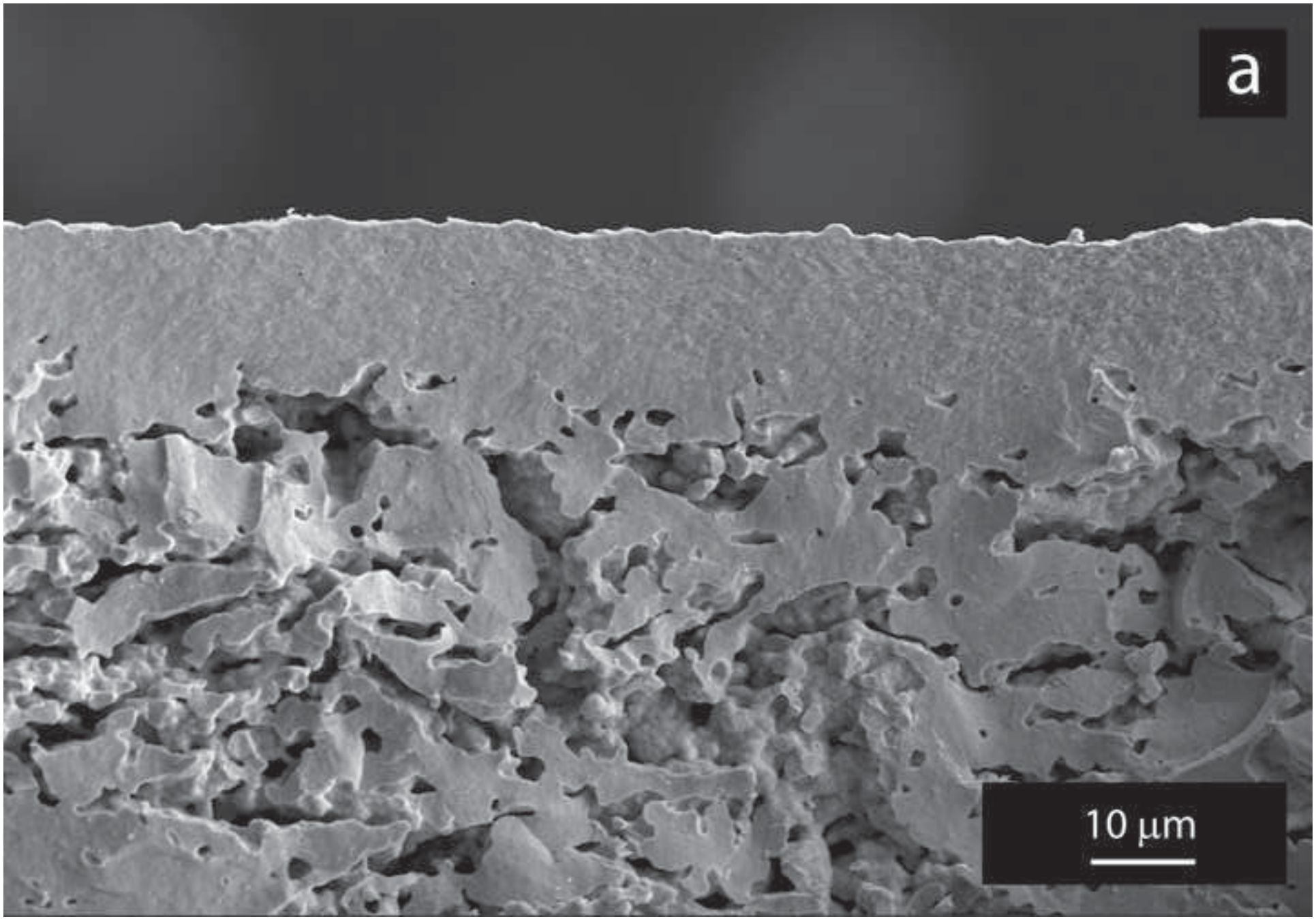

Figure 1b

Click here to download high resolution image

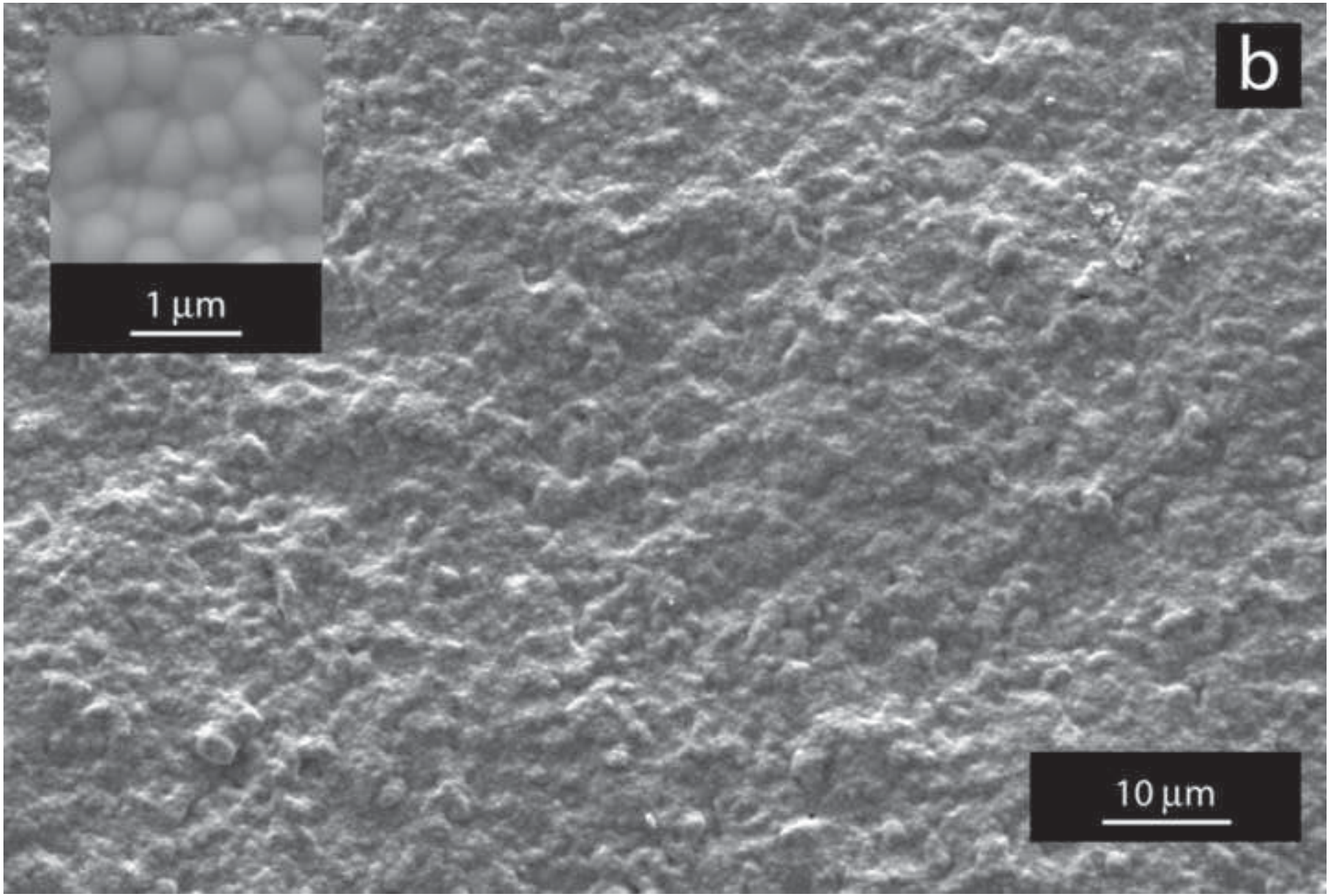

Figure 1c

Click here to download high resolution image

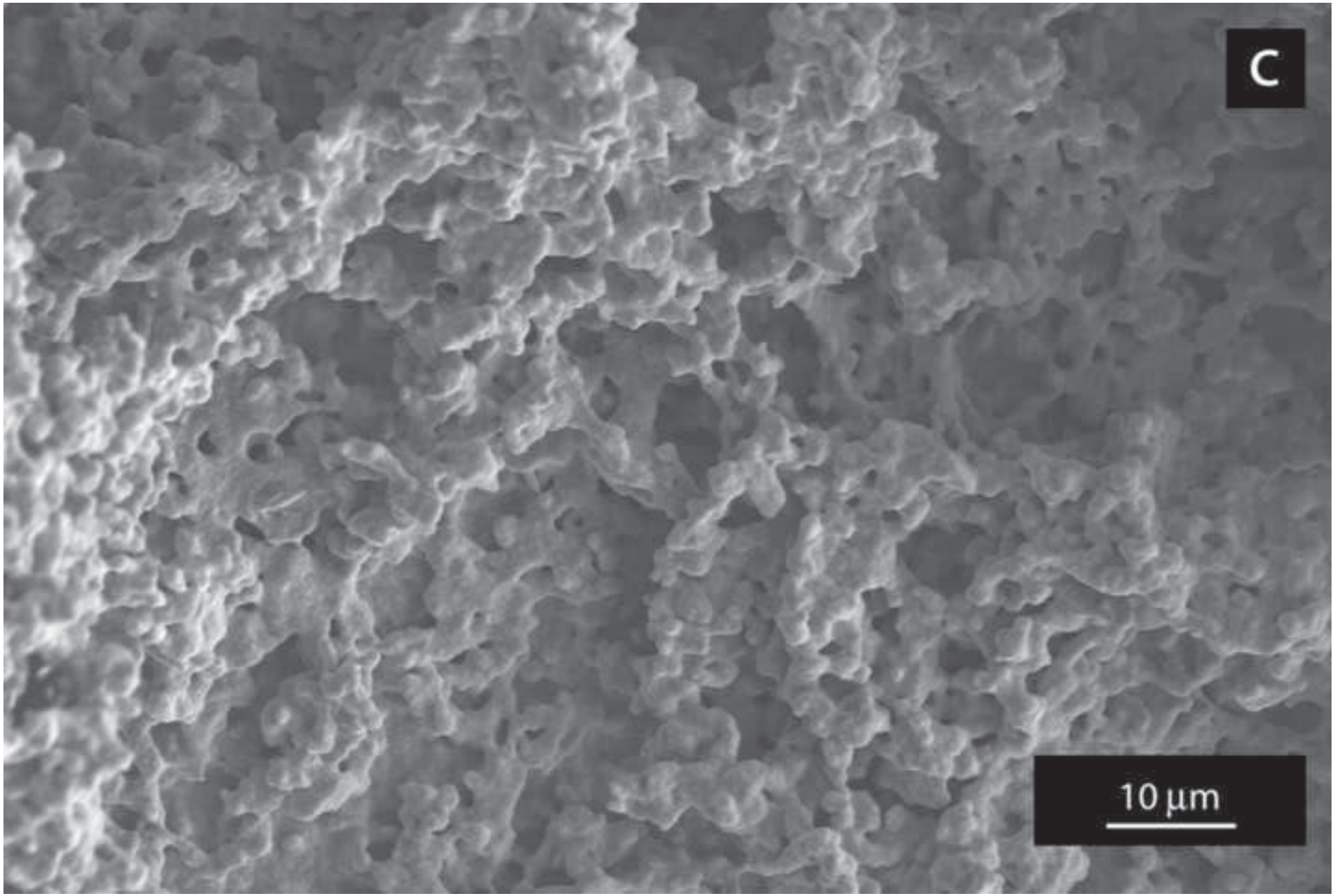

Figure 1d
Click here to download high resolution image

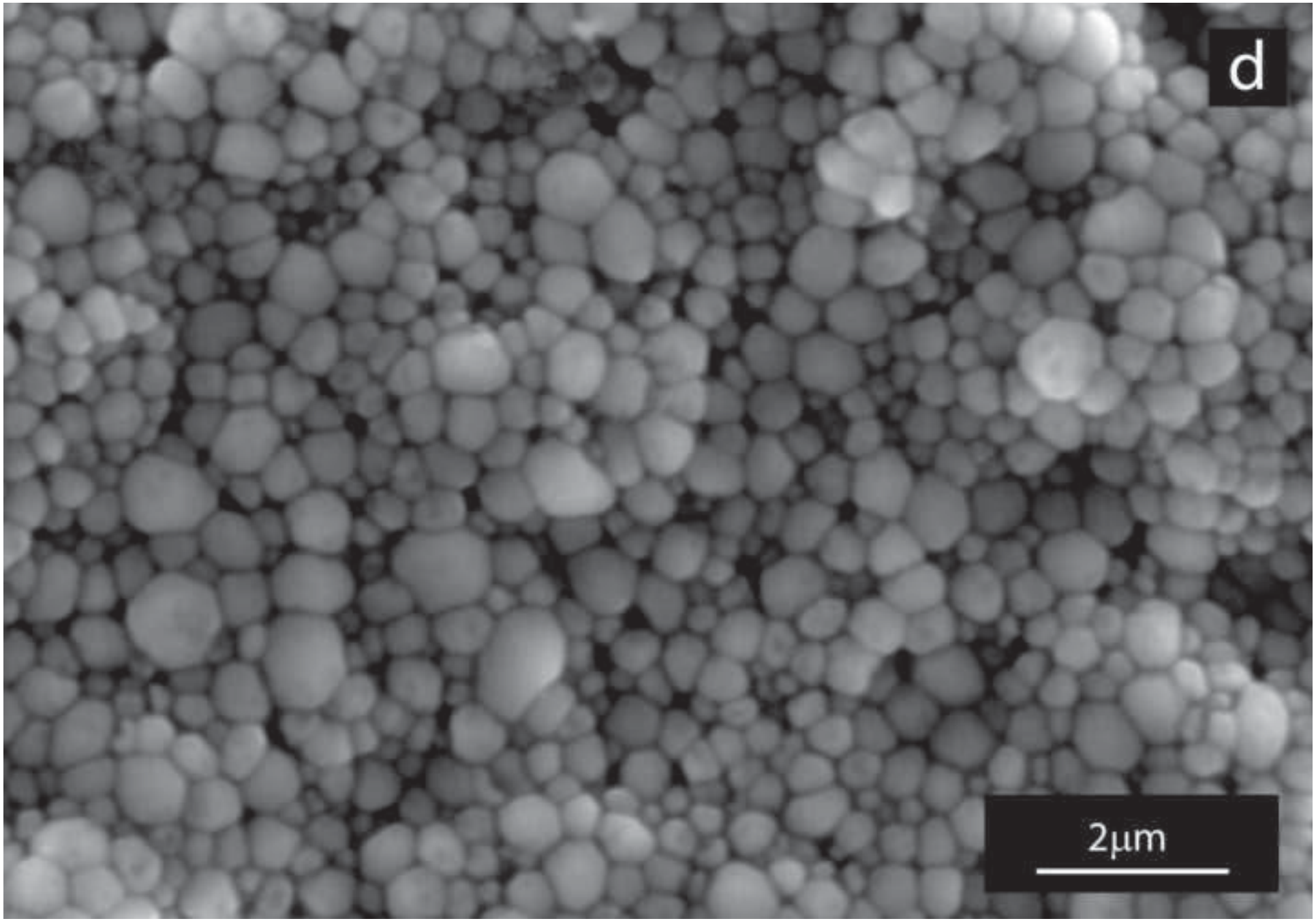

Figure 2a

Click here to download high resolution image

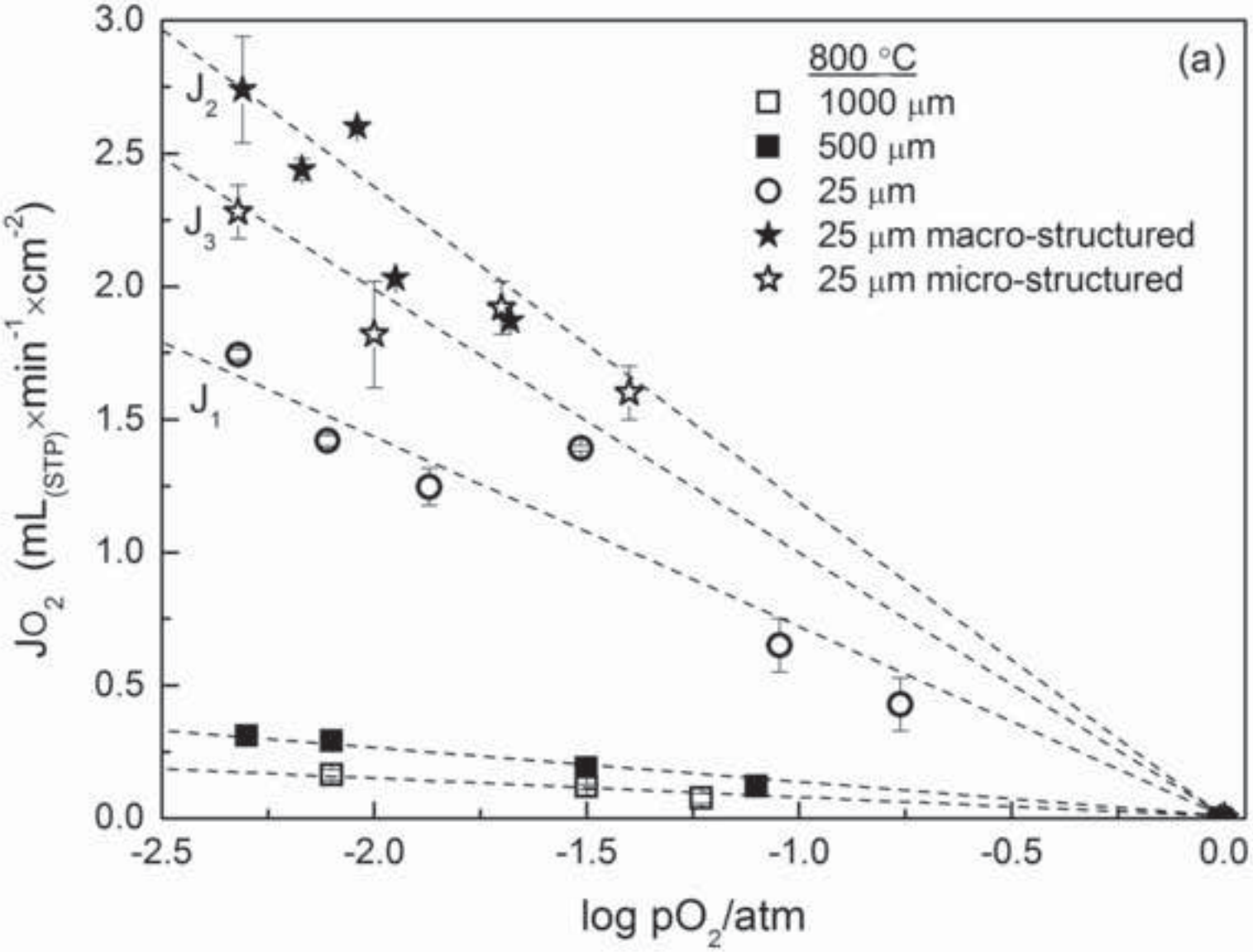

Figure 2b

Click here to download high resolution image

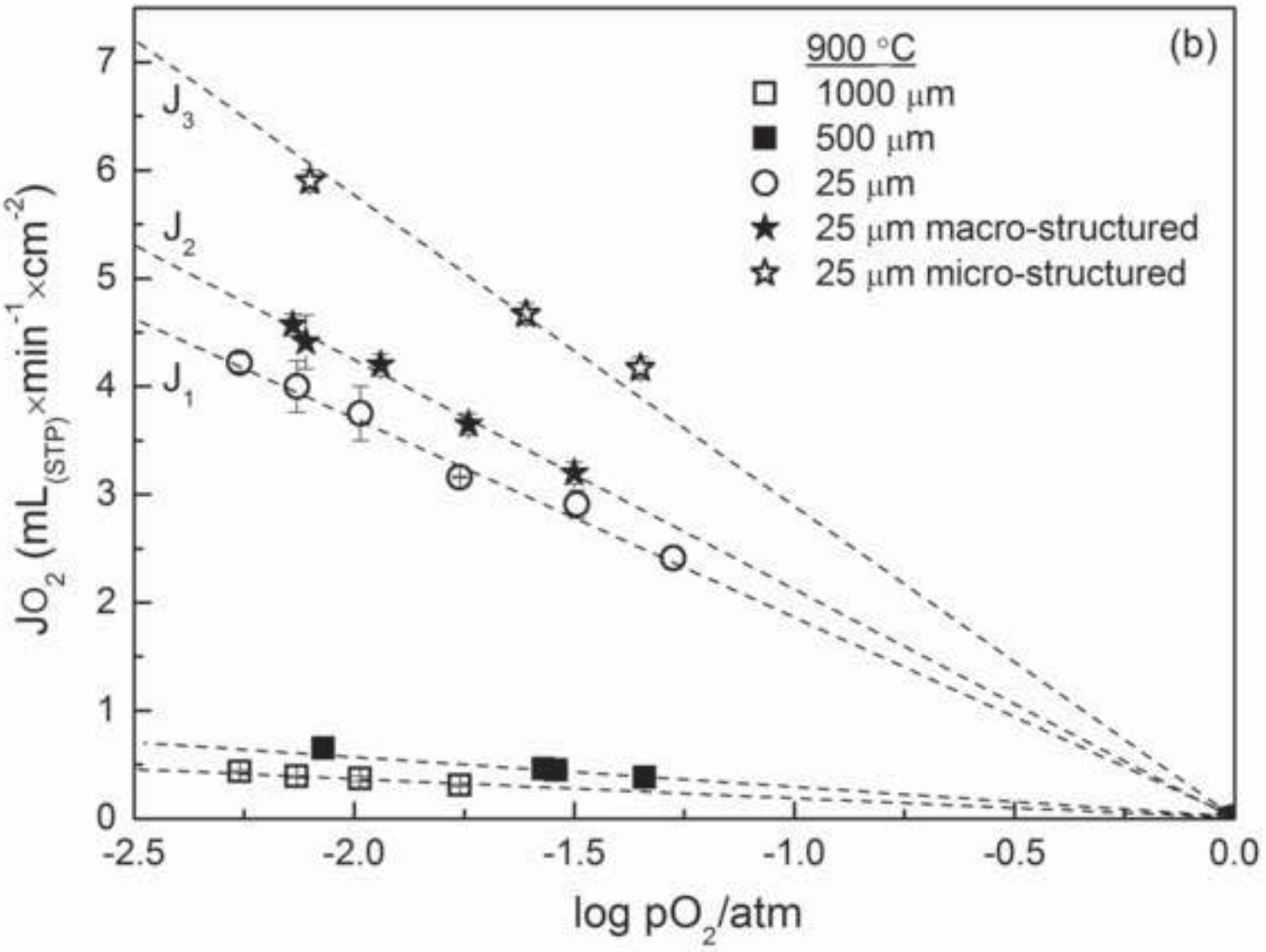

Figure 2c

Click here to download high resolution image

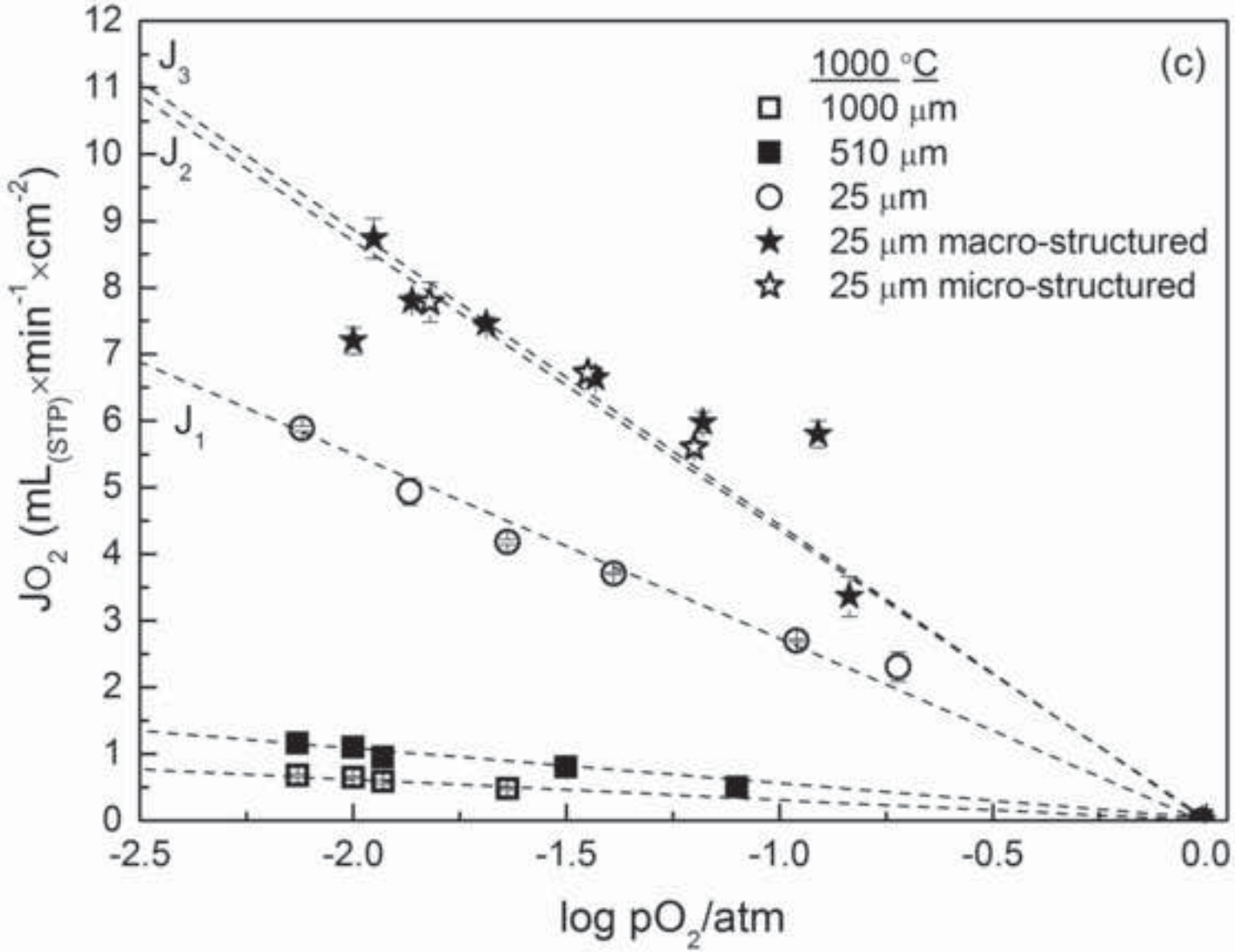

Figure 3

Click here to download high resolution image

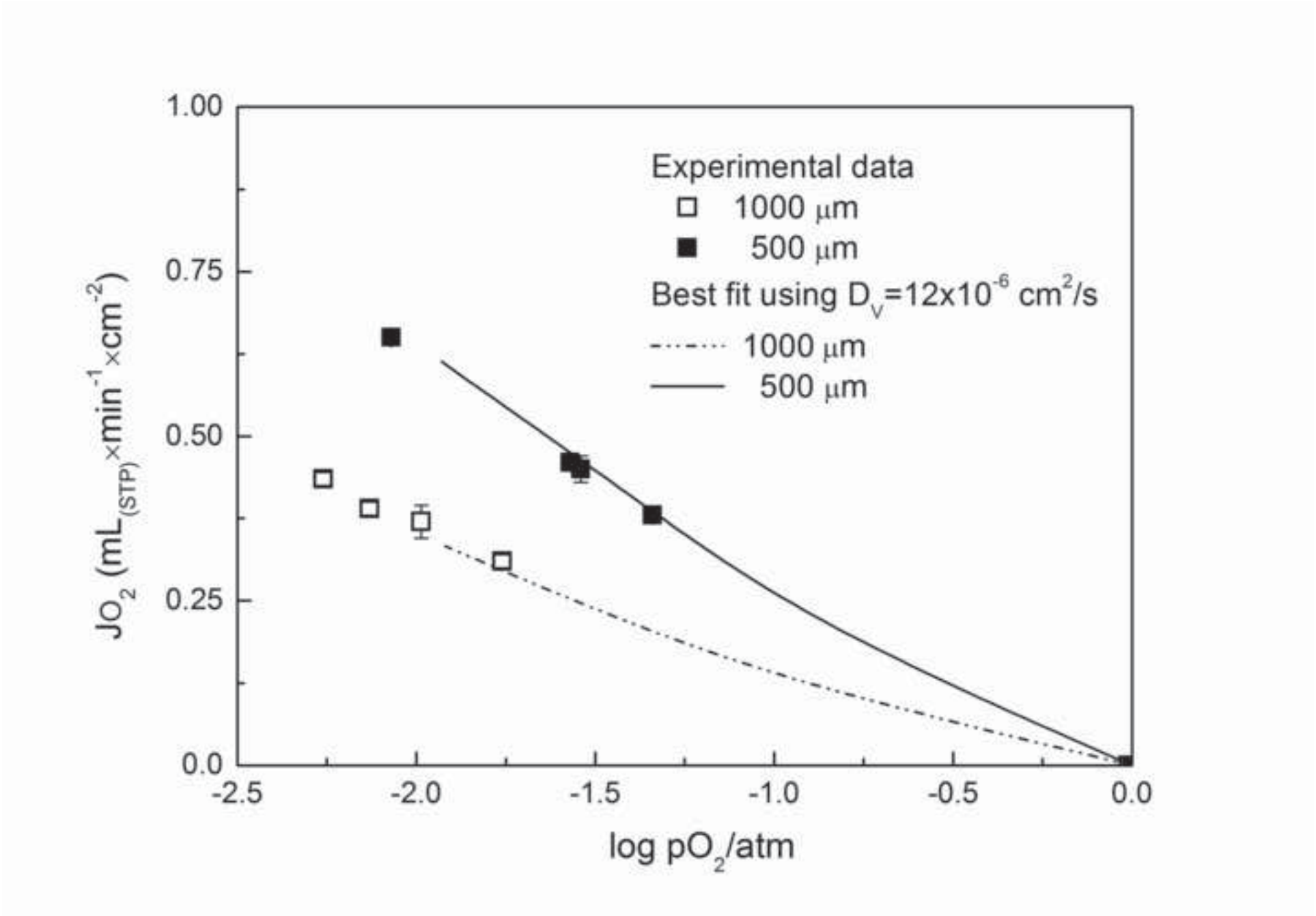

Figure 4

Click here to download high resolution image

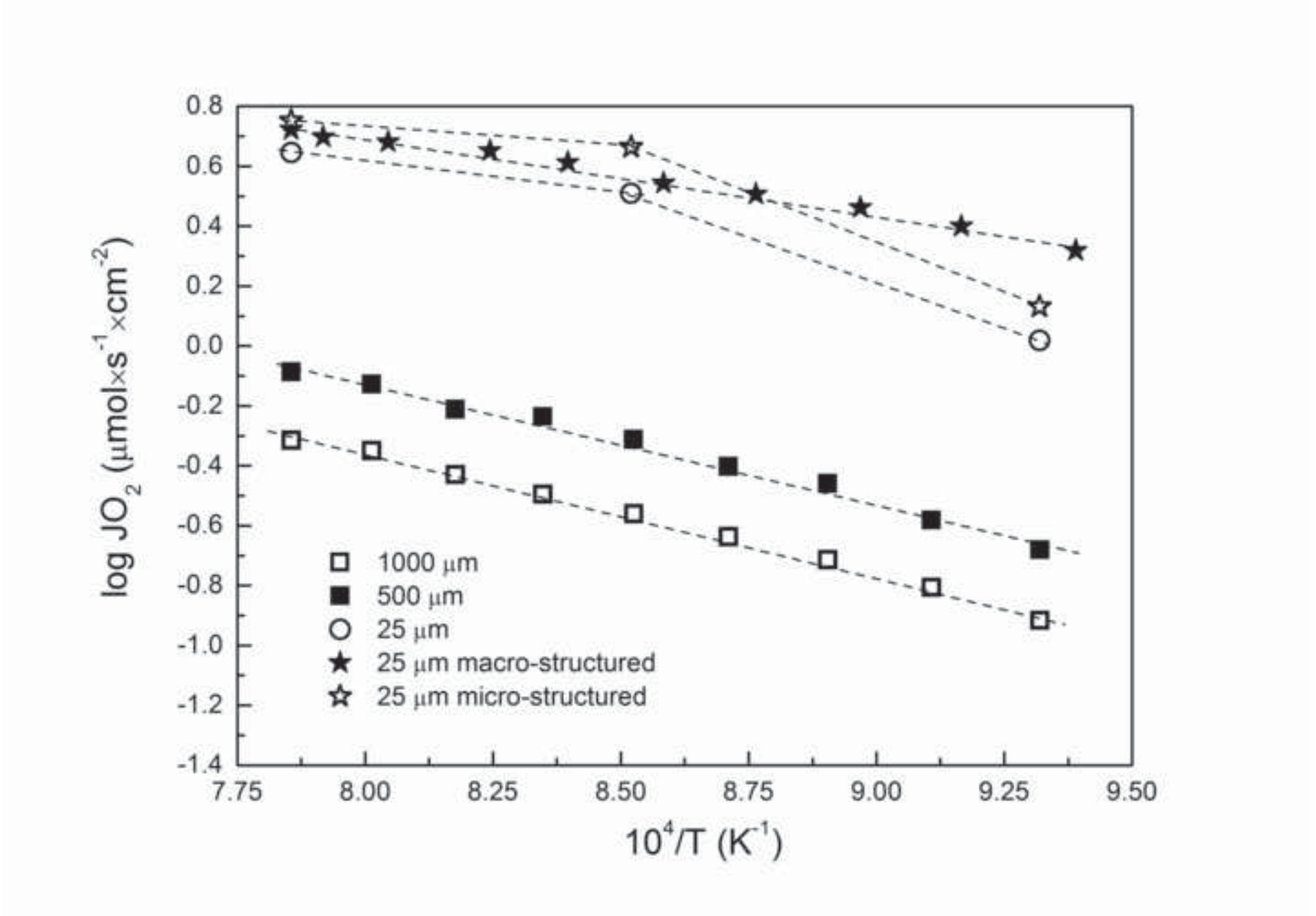

Figure 5

Click here to download high resolution image

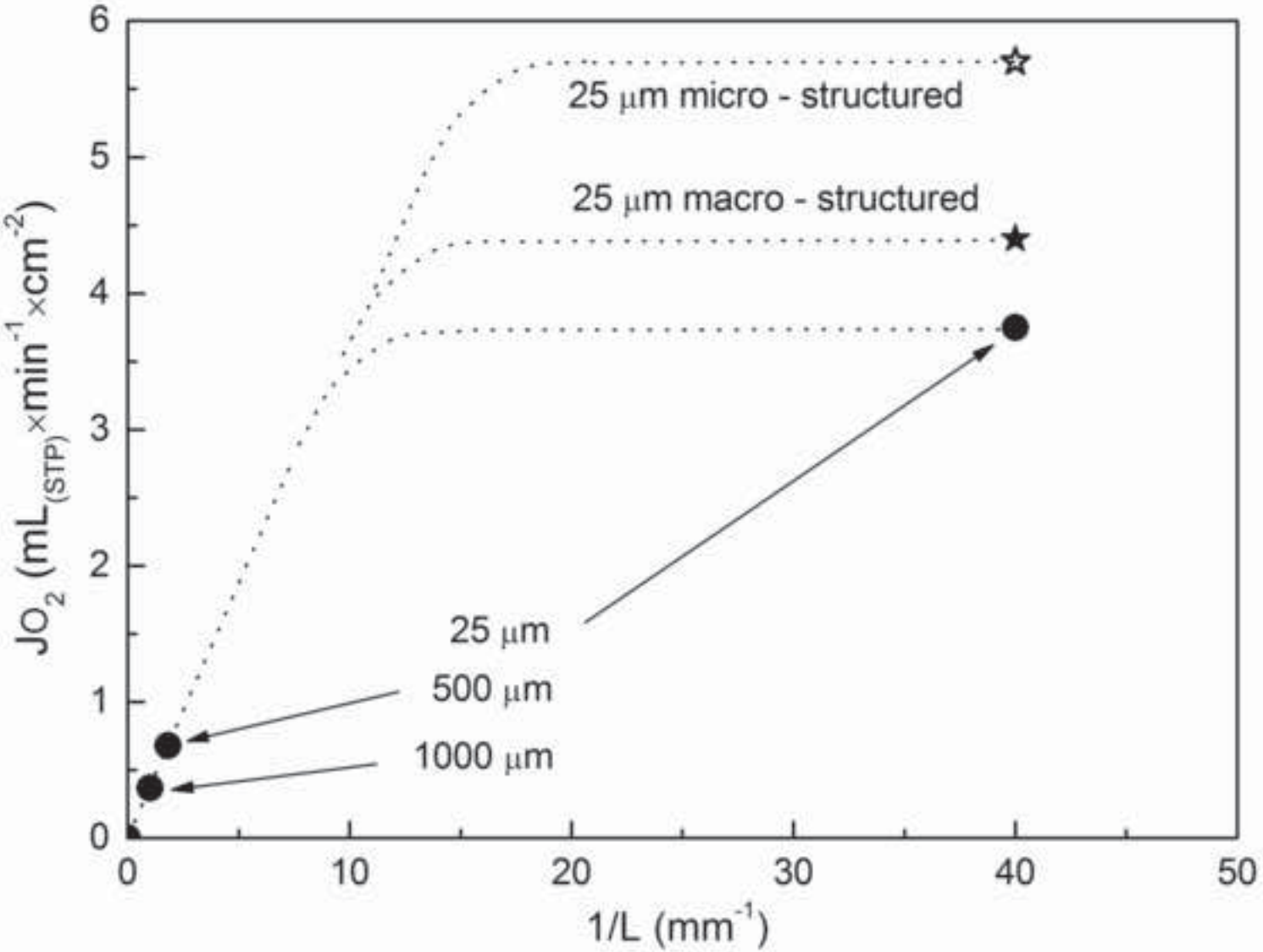

Figure 6a

Click here to download high resolution image

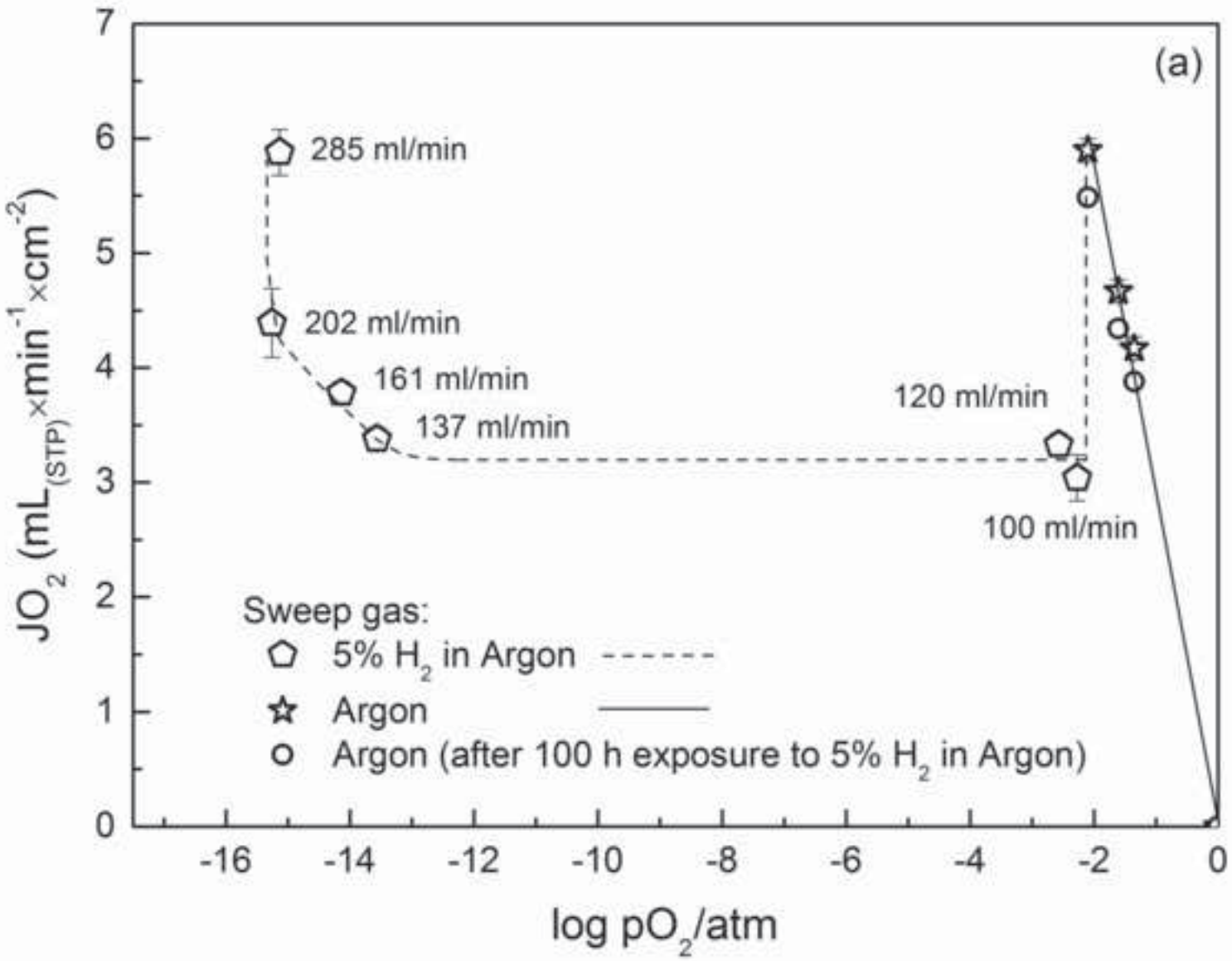

Figure 6b
Click here to download high resolution image

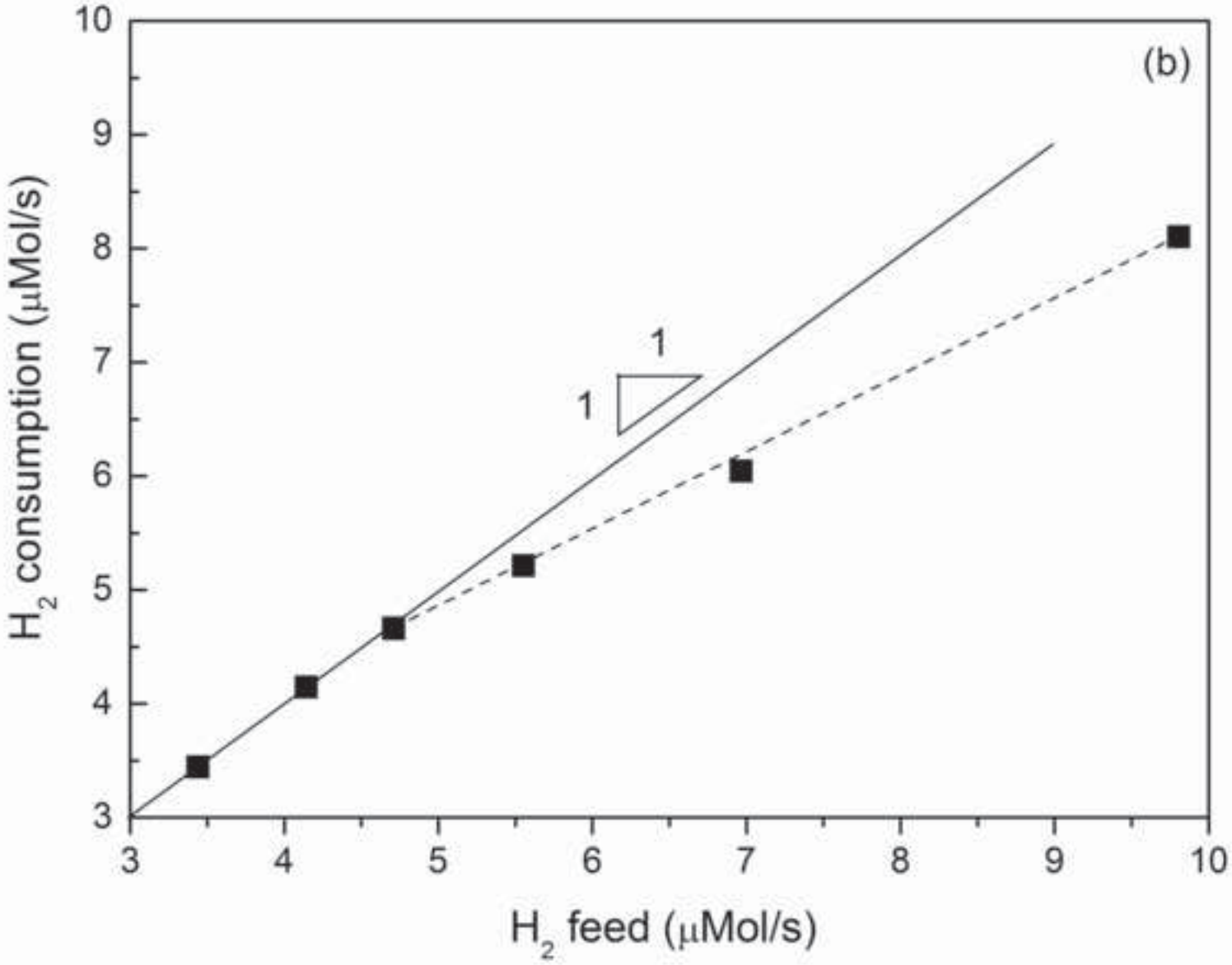

Figure 1. Micrographs (SEM) of as fabricated asymmetric LSFTa membranes: (a) fracture cross section of thin reference membrane, (b) surface of permeate side of thin reference membrane (inclusion shows higher magnification of same surface), (c) surface of permeate side of thin macro-structured membrane and (d) surface of permeate side of thin micro-structured membrane.

Figure 2. Oxygen fluxes versus pO_2 on permeate side of LSFTa membranes with different thicknesses and permeate side modifications: (a) at 800 °C, (b) at 900 °C and (c) at 1000 °C. The dashed lines are a guide to the eye and their intersection (J) with Y axis is used to estimate the ratio of oxygen flux values between asymmetric membranes.

Figure 3. Estimated best fit of oxygen flux values (lines) and experimental data (symbols) versus varying oxygen driving force (partial pressure difference) for thick (500 and 1000 μm) membranes at 900°C.

Figure 4. Arrhenius-type plot showing the natural logarithm of the oxygen fluxes at fixed oxygen partial pressure difference of 10^{-2} atm versus reciprocal absolute temperature. Corresponding apparent activation energy values are summarized in Table 2. The dashed lines are a guide to the eye

Figure 5. Oxygen flux dependence on LSFTa membrane thickness and surface modifications at permeation side at 900 °C and a under fixed oxygen partial pressure difference of 10^{-2} atm. The dashed lines are a guide to the eye.

Figure 6. Performance of LSFTa micro-structured membrane at 900 °C under exposure to H_2 (5% in Argon) sweep gas. Oxygen flux (a) and hydrogen consumption (b) as a function of sweep gas feed. The lines are a guide to the eye.

Figure 7. A post-test micrograph (BSE) and EDS spectrum's of oxygen adsorption side surface of the reference thick membrane (1000 μm). Spectrum 1 (S1) corresponds to the LSFTa phase and spectrum 2 (S2) to the secondary phase.